frontiers in Earth Science

ORIGINAL RESEARCH
published: 02 June 2020
doi: 10.3389/feart.2020.00178

Early Cretaceous Terrestrial Milankovitch Cycles in the Luanping Basin, North China and Time Constraints on Early Stage Jehol Biota Evolution

Wei Liu[1,2], Huaichun Wu[1,2], Linda A. Hinnov[3], Dangpeng Xi[1], Huaiyu He[4], Shihong Zhang[1] and Tianshui Yang[1]*

[1] State Key Laboratory of Biogeology and Environmental Geology, China University of Geosciences (Beijing), Beijing, China, [2] School of Ocean Sciences, China University of Geosciences, Beijing, China, [3] Department of Atmospheric, Oceanic, and Earth Sciences, George Mason University, Fairfax, VA, United States, [4] Institute of Geology and Geophysics, Chinese Academy of Sciences, Beijing, China

This research analyzes the cyclostratigraphy of the lacustrine Dabeigou Formation (DBG) of early Jehol Biota age (~130–135 Ma) in the Luanping Basin, northern China. A high-resolution (2 cm interval), 117.82-m-long magnetic susceptibility (MS) stratigraphic series was measured along the Yushuxia section. MS is positively correlated with thorium, potassium and uranium concentrations associated with gamma ray intensity, and represents a proxy for detrital influx to the Luanping Basin. Power spectral analysis identifies a hierarchy of sedimentary cycles with wavelengths of 16.38 m, 5.85–3.28 m, 1.88–1.33 m, and 0.98–0.7 m, which are interpreted to represent Earth's orbital eccentricity, obliquity and precession index cycles. Objective testing of the MS series supports the interpretation of Milankovitch cycles, indicating an average sedimentation rate of 4.642–4.723 cm/kyr. A floating astronomical time scale with a duration of 2478 kyr is established from interpreted 405 kyr long orbital eccentricity cycles along the MS series. The 405-kyr tuned DBG MS time series closely matches the predicted orbital eccentricity of the La2004 astronomical solution from 130.787 to 133.265 Ma, providing independent temporal constraints on early stage Jehol Biota evolution. Finally, this estimated time interval for the DBG MS time series indicates that it occurred entirely within the Weissert Event.

Keywords: Early Cretaceous, Dabeigou Formation, magnetic susceptibility, astrochronology, Jehol Biota, Weissert Event

OPEN ACCESS

Edited by:
Juan Cruz Larrasoaña, Instituto Geológico y Minero de España, Spain

Reviewed by:
Hong Ao, Institute of Earth Environment, Chinese Academy of Sciences, China
Maodu Yan, Institute of Tibetan Plateau Research, Chinese Academy of Sciences, China

***Correspondence:**
Huaichun Wu
whcgeo@cugb.edu.cn

Specialty section:
This article was submitted to Geomagnetism and Paleomagnetism, a section of the journal Frontiers in Earth Science

Received: *05 January 2020*
Accepted: *06 May 2020*
Published: *02 June 2020*

Citation:
Liu W, Wu H, Hinnov LA, Xi D, He H, Zhang S and Yang T (2020) Early Cretaceous Terrestrial Milankovitch Cycles in the Luanping Basin, North China and Time Constraints on Early Stage Jehol Biota Evolution. Front. Earth Sci. 8:178. doi: 10.3389/feart.2020.00178

INTRODUCTION

The Early Cretaceous terrestrial Jehol Biota in East Asia is well-known for its exceptionally well-preserved feathered dinosaurs, early birds, mammals, pterosaurs, amphibians, insects and early flowering plants, and provides a unique window for understanding the evolution of Early Cretaceous terrestrial ecosystems (Zhou et al., 2003; Zhou, 2014). Geographically, the Jehol Biota is found in the Liaoning Province and adjacent areas in northeastern China. Stratigraphically, it is preserved mainly in the Dabeigou/Huajiying, Dadianzi, Yixian, and Jiufotang formations in ascending order in the Liaoning and Hebei

provinces (**Figure 1**; Xu et al., 2019), with an age range of ∼135–120 Ma (Swisher et al., 1999, 2002; He et al., 2006; Yang et al., 2007; Chang et al., 2009).

It has been increasingly recognized that the biota preserved in the Dabeigou Formation (DBG) reflect the origin and early stage Jehol Biota evolution (e.g., Tian et al., 2004; Ji et al., 2006; Wang and Ji, 2009; Zhou et al., 2009; Huang et al., 2015; Niu et al., 2015; Wang et al., 2015). The discovery of the earliest occurrence of the insect *Ephemeropsis trisetalis* and ostracods in the DBG, together with other fossils, suggests that the earliest Jehol Biota might already have appeared at the time when the lowermost part of Member 2 of the DBG was deposited (Zhou, 2014; Xu et al., 2019). The geochronology of the DBG indicates a range from ∼135 to ∼130 Ma (Liu et al., 2003; Zhang et al., 2005; He et al., 2006; Gao et al., 2018), but has large uncertainties, which impedes further progress in understanding early stage Jehol Biota evolution.

Cyclostratigraphy has been instrumental in establishing a 405-kyr-scale astronomical time scale (ATS) for the Cretaceous Period from well-preserved marine and continental successions (Hinnov, 2018; Huang, 2018). This has been possible due to the stability of the 405-kyr orbital eccentricity cycle over hundreds of millions of years (Laskar et al., 2004, 2011a; Kent et al., 2018). Cyclostratigraphy of the Cretaceous terrestrial strata from the Songliao Basin in northeastern China was interpreted with Milankovitch cycles, and established a ∼28 Myr-long ATS for the upper Turonian-Maastrichtian stages (Wu et al., 2009, 2013a, 2014). Subsequently, Wu et al. (2013b) analyzed cyclostratigraphy of the Lower Cretaceous Yixian Formation in the Sihetun Basin, northeastern China, estimating an average sedimentation rate of ∼1.70 cm/kyr for the Jianshangou Beds that host "feathered" dinosaur/primitive bird fossils of the Jehol Biota. Most recently, Liu et al. (2020) found that the cyclic alluvial-fluvial synrift deposits of the Lower Cretaceous (Valanginian-Hauterivian) Shahezi Formation in Songliao Basin were controlled by astronomical forcing, and reconstructed an ∼11.14 Myr-long floating astrochronology based on interpreted 405-kyr cycles.

The Lower Cretaceous DBG in the Yushuxia section, Luanping Basin (LPB), Hebei Province, the focus of this study, consists of 213 m of dominantly cyclic continental strata in well-exposed outcrops with abundant fossils (Liu et al., 2002; Tian et al., 2004; Wu et al., 2004; Zhang et al., 2007; Zhou et al., 2009; Niu et al., 2010). It provides a unique opportunity to develop an astrochronology to enable characterization of terrestrial climate change and environmental evolution of the Early Cretaceous Period. In this study, we conducted detailed time series analysis and modeling of the high-resolution (2 cm interval) magnetic susceptibility (MS) series of the DBG. The objectives were to search for and identify astronomical signals in the DBG, to develop an astrochronology for the early stage Jehol Biota, and to test the reliability of the astronomical solutions for early Cretaceous time.

GEOLOGICAL SETTING

The Luanping Basin (LPB) is located in northeastern Hebei Province, northern China, near the northern margin of the Yanshan orogenic belt (**Figure 1**). The paleo-latitude of LPB was ∼40° N during the Cretaceous Period, i.e., approximately the same as today (Wang, 2013; Wang C. S. et al., 2013). Here, the Volcanic Sedimentary Basin Group was formed by the active tectonics and frequent volcanic eruptions during the Late Jurassic to Early Cretaceous (Tian et al., 2004). The LPB is one of the small, terrestrial extensional basins in the Yanshan structural belt with a complete sedimentary sequence (Wu et al., 2004; Zhang et al., 2007). Its sedimentary evolution involved three successive stages: (1) "vigorous volcanic eruptions," (2) "extensional subsidence," and (3) "sedimentary infilling" (Zhang et al., 2007). The Jurassic and Cretaceous terrestrial strata in LPB are divided into six lithologic formations (in descending order): Jiufotang, Xiguayuan, Dadianzi, DBG, Zhangjiakou and Houcheng formations (Tian et al., 2008; Wang and Ji, 2009; Wang S. E. et al., 2013).

The DBG of the 213 meter-thick Yushuxia section (**Figure 1**) is well-known for its continuous non-marine Lower Cretaceous deposits and preservation of early stage Jehol Biota, including plants, pollen, spores, spinicaudatans, gastropods, bivalves, ostracods, insects, and fishes (Liu et al., 2002; Tian et al., 2004; Li et al., 2004; Zhou et al., 2009; Wang et al., 2015). The stratigraphy is characterized by alternating deposition of mudstones, shales, and siltstones, interbedded with sandstones and conglomerates of semi-deep lake facies in the lower part and deep lake facies in front of fan deltas in the upper part (**Figure 2**; Liu et al., 2001; Wang and Ji, 2009).

The DBG is divided into 3 members and 46 layers according to a detailed description of sedimentology and stratigraphy (Li et al., 2004; Qin et al., 2018). Member 1 (49.39 m) consists of tuffaceous, pebbly and coarse-grained sandstones, and medium to fine-grained sandstones intercalated with tuffaceous siltstone, sedimentary tuff and thin volcanic ashes. Member 2 (98.44 m) consists of siliceous mudstones and shales, interlayered with siltstones, fine to medium-grained sandstones; abundant fossils occur in this member. Member 3 (76.68 m) consists of mudstones, silty mudstones, calcareous mudstones and pelitic siltstones, and abundant fossils. The DBG represents shoreline-shallow lake to fan delta front-semi-deep lake facies in the lower part, and deep lake to fan delta front facies in the upper part (Liu et al., 2001).

The age of the DBG has been disputed for a long time. The paleontological data, including ostracods, spinicaudatans, palynotaxa, and plant macrofossils indicate that the DBG ranges from Late Jurassic to Early Cretaceous (e.g., Wan et al., 2016; Qin et al., 2018; Xi et al., 2019). Radioisotopic dating provides further constraints: in the Yushuxia section, SHRIMP zircon U-Pb dating of the tuffs in Layers 34 and 21, and the volcanic rocks of the underlying Zhangjiakou Formation indicates ages of 133.9 ± 2.5 Ma, 129.9 ± 1.2 Ma, and 135.4 ± 1.6 Ma, respectively (**Figure 2**; Liu et al., 2003; Gao et al., 2018). Zhang et al. (2005) obtained a LA-ICP-MS zircon U-Pb age of 135.2 ± 2.3 Ma from the Zhangjiakou Formation in the same section (**Figure 2**). $^{39}Ar/^{40}Ar$ dating of a tuff layer in the upper DBG of the Jiecaigou section, near LPB, yielded an age of 130.7 ± 1.2 Ma (He et al., 2006). Thus, the DBG can be constrained roughly from ∼135 to ∼130 Ma. The most recent constraints for Valanginian-Hauterivian time

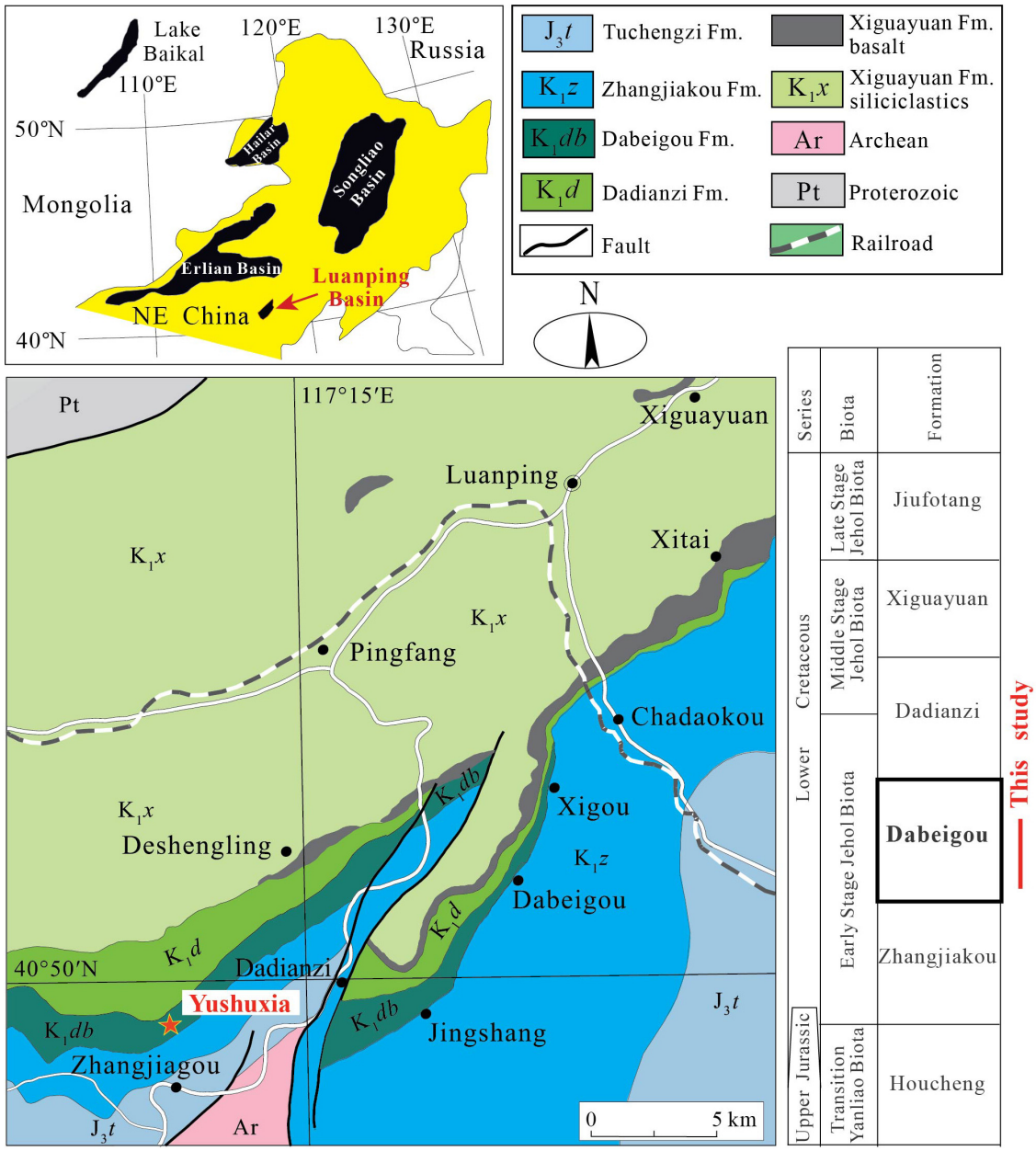

FIGURE 1 | Left: Map of northeastern China, Songliao Basin (SLB), and Luanping Basin (LPB), modified from Qin et al. (2018). The location of the Yushuxia section is indicated with the red star, at GPS coordinates 40°47′ N, 117°12′ E. Right: Lower Cretaceous stratigraphic column of northern China indicating the evolution stages of the Jehol Biota. The Dabeigou Formation is highlighted with bold lines; the stratigraphic coverage of this study is shown by the vertical red line at the far right.

are: 126.08 ± 0.19 Ma (top Hauterivian) 131.29 ± 0.19 Ma (top Valanginian); and 137.05 ± 1.0 Ma (top Berriasian) (Martinez et al., 2015; Aguirre-Urreta et al., 2019), which indicates that the DBG corresponds to late Valanginian to early Hauterivian time.

DATA

Magnetic susceptibility (MS) is a measure of the degree of magnetization of a material when subject to an external magnetic field. In sediments and sedimentary rocks, MS is affected by the concentration, grain size and shape of magnetic minerals (Kodama, 2012). Many studies have shown that MS is an effective indicator for Milankovitch-scale signals in stratigraphy, and it has been extensively used to characterize both marine and terrestrial sediments (e.g., Wu et al., 2013b; Zhong et al., 2018; Kodama, 2019).

MS was measured at 0.02 m intervals (on average) along the recently exposed Yushuxia section using a portable SM-30 MS detector. A total of 117.82 meters was measured, for a total of

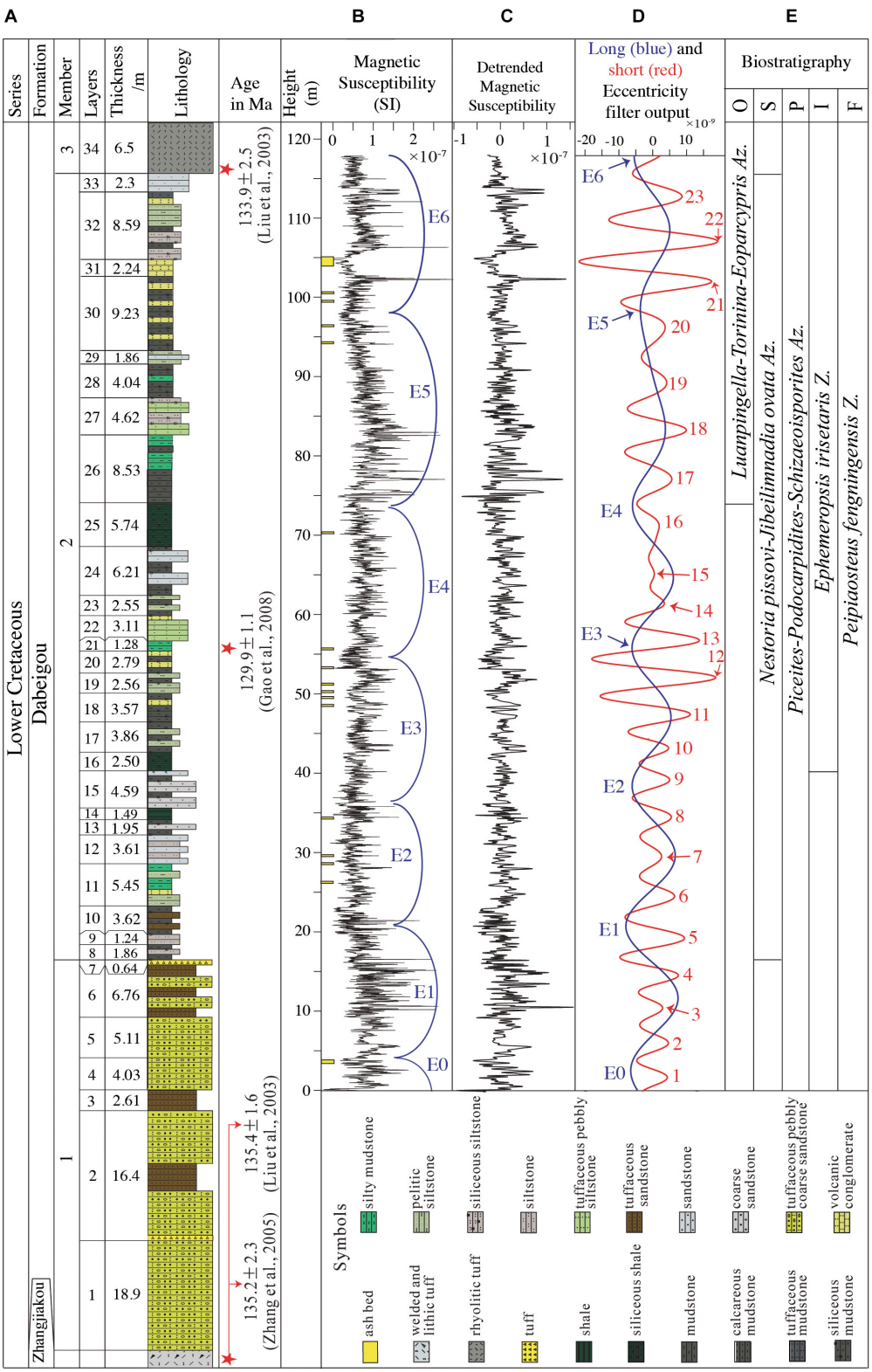

FIGURE 2 | MS series of the DBG section. **(A)** The detailed measured section with numbered beds and U-Pb ages (modified from Qin et al., 2018). **(B)** The MS series with interpreted long orbital eccentricity (E0-E6) cycles. **(C)** Detrended MS series. **(D)** Long (blue) and short (red) orbital eccentricity Gaussian filter outputs with passbands of 0.053 ± 0.01 and 0.2 ± 0.05 cycles/m, respectively. **(E)** Biostratigraphy from Qin et al. (2018). O, ostracods; S, spinacaudatans; P, palynotaxa; B, bivalves; I, insects; F, fishes.

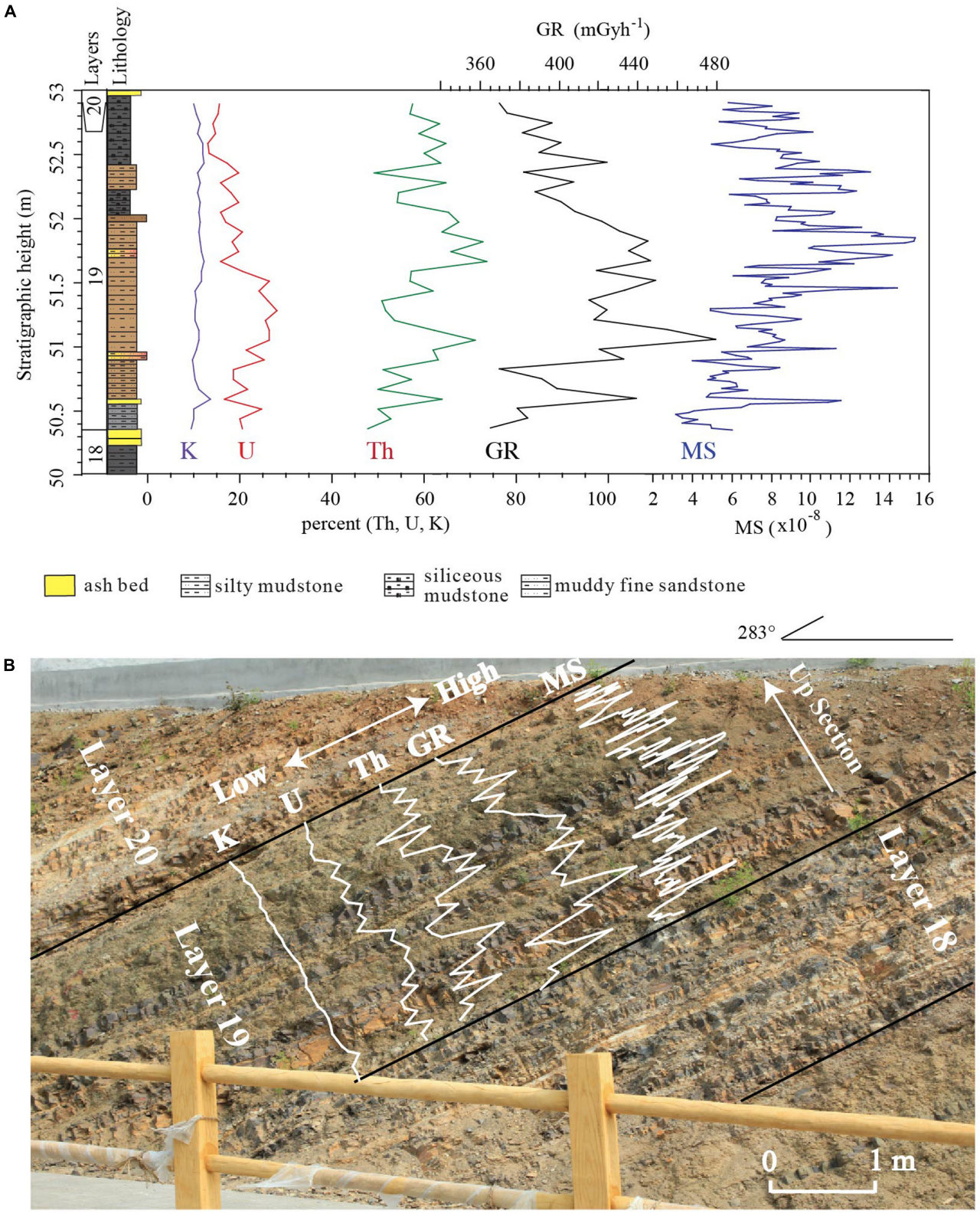

FIGURE 3 | (A) Comparison of lithology, MS, gamma ray (GR) intensity, and percent (%) of Th, K and U contributions in Layer 19. **(B)** Outcrop photo of Layers 17–20 with *in situ* measured data from Layer 19.

TABLE 1 | Orbital eccentricity, obliquity, and precession index periodicities from the periodogram of the La2004 astronomical solution (Laskar et al., 2004), between 129.55 and 134.55 Ma, i.e., a 5 Myr-long interval with a median age 132.05 Ma, calculated by Acycle for the TimeOpt astronomical target (orbital eccentricity and precession index) and for the ASM and COCO astronomical frequency targets (all three astronomical parameters).

Astronomical parameter	Periodicity (kyr)
Orbital eccentricity	409.6000
	132.1290
	124.1212
	99.9024
	94.1609
Obliquity	36.6000
Precession index	21.1405
	20.9514
	18.0839
	17.9256

Frequency in cycles/kyr is obtained by 1/periodicity.

5892 data points. This MS stratigraphic series covers from the top part of Member 1 (Layers 4–7; 16.54 m), Member 2 (Layers 8–33; 99.39 m) and the lower part of Member 3 (Layer 34; 1.89 m) (**Figure 2B**). Gamma ray intensity was measured at 0.1 m intervals along the section using a portable RS-230 GR detector; in this study measurements are presented for Layer 19 only for comparison (**Figure 3**).

MATERIALS AND METHODS

Pre-processing

The Prior to analysis, the data of 16 ash beds was removed, and MS series was interpolated to the average sample rate of 0.02 m. A low-pass filter was applied to the MS stratigraphic series using *tanerfilter.m* to retain astronomical frequencies while removing the very high frequencies. A cut-off frequency of 5 cycles/m and roll-off rate of 10^{12} were defined to reject wavelengths shorter than 0.2 m. The low-pass filtered MS series was then smoothed with a 40-meter-long window with the Matlab function *smooth.m* with the "lowess" option to estimate irregular long-term trends that could interfere with the detection of low frequency orbital eccentricity cycles. This smoothed curve was then subtracted from the MS series (**Figure 2C**).

Spectral Analysis

Multi-taper method (MTM) power spectral analysis (Thomson, 1982) with *pmtm.m*, and the evolutionary Fast Fourier Transform (FFT) spectrogram with *evofft.m* (Kodama and Hinnov, 2015) were used to characterize the frequency content of the processed MS series. The MTM F-ratio test was used to determine significant harmonic lines. The MTM harmonic *F*-test used in the average spectral misfit analysis (see below) was performed using the "eha" function of the Astrochron package in R (Meyers, 2014); otherwise *F*-test significance values were computed with Acycle (Li et al., 2019). The application of frequency ratios, e.g., 20:5:2:1 for long orbital eccentricity (405 kyr), short orbital eccentricity (100 kyr), obliquity (36.6 kyr), and precession (20 kyr) served as a preliminary test for astronomical frequencies in the MS stratigraphic series (Huang et al., 1992; Mayer and Appel, 1999; Laskar et al., 2004).

Sedimentation Rate Modeling

Three objective methods were used to test jointly for the presence of astronomical frequencies and the most probable sedimentation rate for the DBG MS stratigraphic series:

1. Average spectral misfit (ASM) analysis (Meyers and Sageman, 2007) estimates an optimal sedimentation rate given a set of astronomical target frequencies that is compared with the set of statistically significant frequencies of the stratigraphic data series for a specified range of sedimentation rates. The sedimentation rate with the lowest misfit between data and target frequencies is the "optimal sedimentation rate" (**Supplementary Material**).
2. Time Optimization (TimeOpt) analysis evaluates orbital eccentricity-like variations in the data, together with supporting evidence from amplitude modulations of the precession index band, across a test range of sedimentation rates (Meyers, 2015, 2019). TimeOptSim performs Monte Carlo AR1 model simulations to evaluate significance of TimeOpt results (Meyers and Malinverno, 2018; **Supplementary Material**).
3. Correlation coefficient (COCO) analysis (Li et al., 2018) estimates the correlation coefficient between power spectra of a stratigraphic proxy series and an astronomical solution in the time domain for a range of sedimentation rates. The evolutionary correlation coefficient (eCOCO) procedure was used to investigate changes in sedimentation rate along the stratigraphic series (Li et al., 2018). COCO and eCOCO analysis with 5000 Monte Carlo simulations was performed on test sedimentation rates ranging from 1 to 10 cm/kyr (**Supplementary Material**).

The ASM procedure was carried out using the Astrochron package in R (Meyers, 2014); TimeOpt, TimeOptSim, COCO, and eCOCO procedures were performed using the software ACycle v 2.1 (Li et al., 2019). The astronomical target frequencies used in these three procedures are based the La2004 astronomical solution periodogram for the 5-myr-long interval 129.55–34.55 Ma (median age of 132.05 Ma) (**Table 1**; Laskar et al., 2004).

The La2004 Astronomical Solution

The accuracy of astronomical solutions declines rapidly prior to 50 Ma, and solutions other than the well-known La2004, e.g., La2010 and La2011, are thought to incorporate parameterizations and initial conditions that are superior to those used in La2004 (Laskar et al., 2011a,b), and more closely fit geological data around and prior to 50 Ma, e.g., La2010c and ZB18a (Zeebe and Lourens, 2019). The main issue centers on modeling the fundamental frequencies that involve the orbits of Earth (g_3, s_3) and Mars (g_4, s_4), and the expectation for chaotic interactions

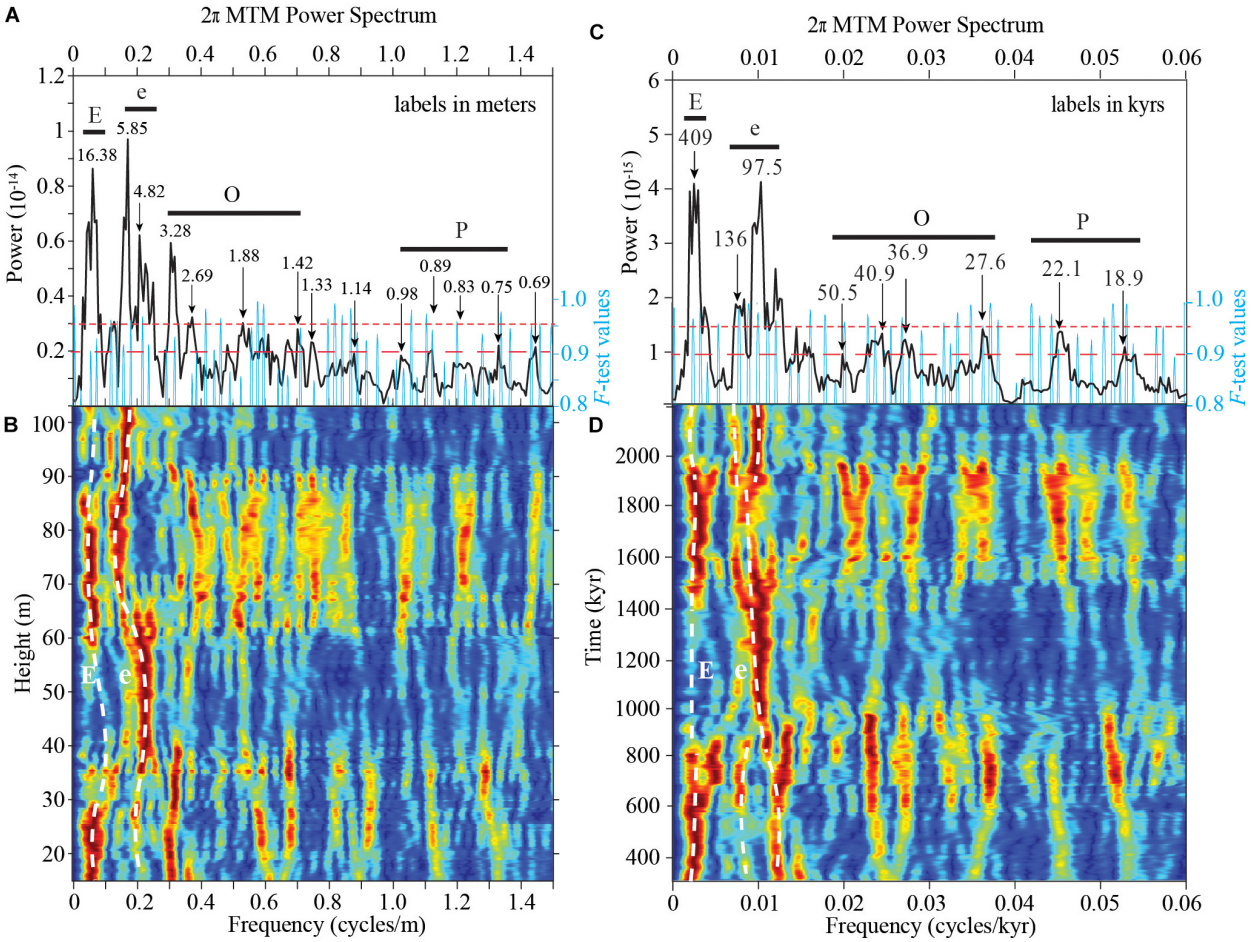

FIGURE 4 | Spectral analysis of the DBG MS stratigraphic series and 405-kyr-tuned series, frequency range: f = (0, 1.5 cycles/m) and f = (0, 0.06 cycles/kyr). **(A)** 2π MTM power spectrum of MS stratigraphic series with F-test values for significant harmonic lines. **(B)** Evolutionary FFT spectrogram of MS stratigraphic series with a 30 m sliding window. **(C)** 2π MTM power spectrum of 405-kyr-tuned MS series with F-test significance values for harmonic lines. **(D)** Evolutionary FFT spectrogram of 405-kyr-tuned MS series with a 600 kyr sliding window. E, long orbital eccentricity; e, short orbital eccentricity; O, obliquity; P, precession index.

between these two planetary orbits through deep time. For example, La2004 from 92 to 90 Ma and 87 to 85 Ma, predicts chaotic transitions between the Earth and Mars orbits. Recently, it was discovered that these two transitions closely fit Late Cretaceous cyclostratigraphic patterns from the Western Interior Seaway (Ma et al., 2017, 2019). Here we will test whether the La2004 solution also fits cyclostratigraphic patterns of the Early Cretaceous time represented by the DBG.

RESULTS

MS Variations

MS values range from -2.4×10^{-8} SI to 4.2×10^{-7} SI, with an average of 7.02×10^{-8} SI (**Figure 2B**). The MS stratigraphic series shows a sustained cyclic pattern that is consistent with the decimeter- to meter-scale lithological cycles (**Figures 2**, **3**). MS is positively correlated with gamma ray intensity and elevated ^{232}Th, ^{40}K, and ^{238}U (**Figure 3**). Th contributes ∼60% of the GR signal, which identifies GR as a primarily clay proxy ("shale log") (Crain, 2019) that tracks the detrital influx from surrounding terrestrial source areas (Ohta et al., 2011). Recently, Pei et al. (2019) identified primary magnetic remanence and constructed a magnetostratigraphic framework for the upper DBG in LPB, further supporting the validity of the MS series as an important paleoenvironmental and paleoclimatic proxy. We propose that DBG MS is a proxy for the terrestrial hydrologic cycle, weathering and fluvial intensity, and if these processes were forced by insolation, represent Milankovitch cycles.

The DBG Stratigraphic Spectrum

2π MTM power spectral analysis of the MS stratigraphic series indicates spectral peaks at wavelengths of 16.38 m, 5.85–4.82 m, 3.28–1.42 m, and 0.98–0.7 m above the 90% F-test value (**Figures 4A,B**). The ratio of the major cycle bands of 20.5–16.4 m: 5.85–4.82 m: 3.28–1.42 m: 0.98–0.7 m is similar to the ratio of the Early Cretaceous astronomical periodicities of long orbital eccentricity (405 kyr) : short orbital eccentricity (132, 124, 99, and

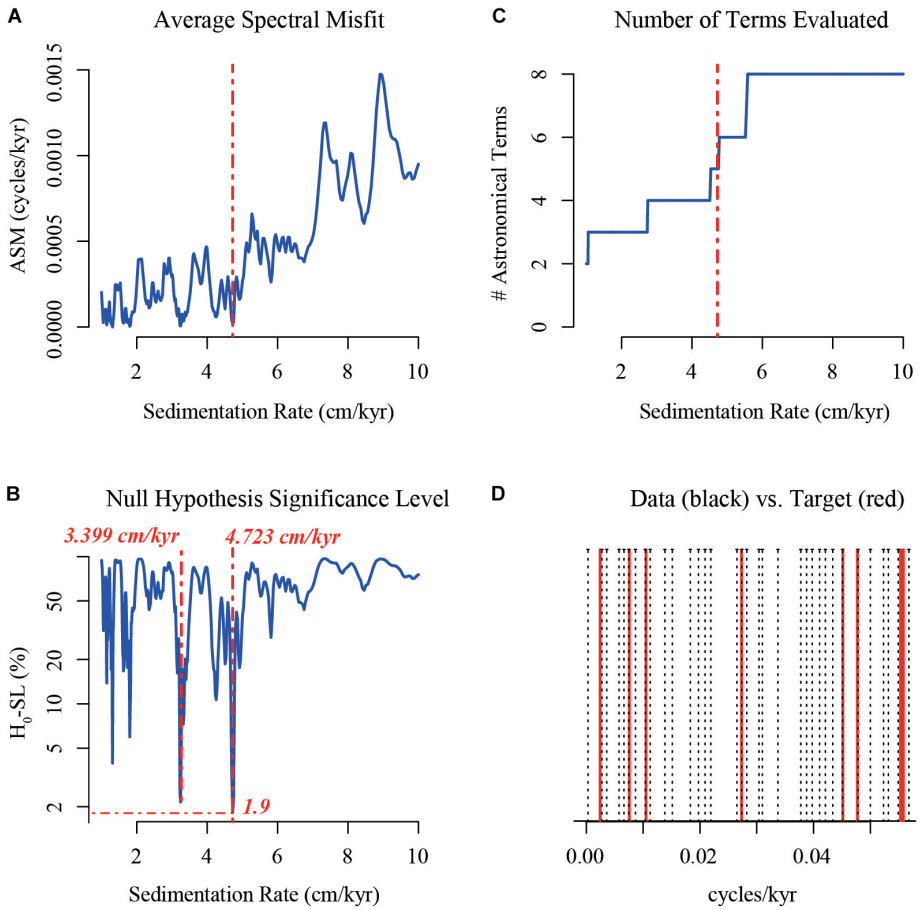

FIGURE 5 | ASM analysis of the DBG MS series, applied over a range of sedimentation rates from 1 to 10 cm/kyr by 0.0225 cm/kyr steps, using the La2004 astronomical target frequencies for 129.55–134.55 Ma (**Table 1**). All harmonics in the MS series exceeding 85% significance level, a total of 42, are evaluated. The astronomical target used is based on the list in **Table 1**, but has reduced the number of short eccentricity terms from four (1/132.129, 1/124.1212, 1/99.9024, 1/94.1609) to two (1/132.129, 1/95.25), which was found to yield a significantly lower H_0 (see **Supplementary Material** for ASM analysis with all 10 terms). **(A)** The ASM statistic between data and target spectrum. **(B)** The results of null hypothesis testing: H_0 is the probability of no target astronomical frequencies in the data. The optimal sedimentation rate occurs at the first joint lowest value ASM statistic and statistically significant H_0 minimum in the tested sedimentation rate range. **(C)** The number of astronomical terms used in the statistic; a total of 8 terms (frequencies) are included in the target (see above). **(D)** Comparison of significant spectral lines (dotted black lines) evaluated at the optimal sedimentation rate identified in **(C)** and the astronomical target lines (solid red lines). Vertical dash-dot red lines indicate solutions for optimal sedimentation rates.

95 kyr) : obliquity (37 kyr) : precession (23.0, 22.5, 21.8, 18.7, and 18.5 kyr) (Laskar et al., 2004). These cycles may be correlated with Milankovitch cycles of short orbital eccentricity, obliquity and precession according to the cycle length ratios. The evolutionary FFT spectrogram of the MS stratigraphic series (**Figure 4A**) indicates a sudden shift of power to higher frequencies in the 35–65 m interval, followed at ∼65 m by an equally sudden shift back to the lower frequencies that is then maintained to the base of the series. The question is whether these shifts indicate sudden changes in sedimentation rate, or evolution of the astronomical frequencies.

Sedimentation Rate Optimization

ASM Analysis

ASM analysis indicates a statistically significant (H0∼1%) solution at 4.723 cm/kyr (**Figure 5**). However, only five of the total of eight astronomical target frequencies were evaluated for this result, with the long orbital eccentricity at 409.6 kyr, and short precession index terms at 18.08 and 17.9256 kyr not successfully fitted to within the half-Rayleigh spacing required by the ASM statistic (Equation 1 in Meyers and Sageman, 2007), as indicated by three vertical red lines that do not coincide with any of the black vertical dashed lines in **Figure 5D**.

TimeOpt/TimeOptSim Analysis

TimeOpt analysis (**Figure 6**) indicates a r^2_{opt} maximum at a sedimentation rate of 4.642 cm/kyr, for which TimeOptSim analysis estimates a *p*-value of 0.119 (**Figure 6I**). This is close to the 4.723 cm/kyr sedimentation rate solution obtained by ASM (see above). The $r^2_{envelope}$ assessment (**Figure 6A**) indicates a much faster 9.224 cm/kyr with a very low *p*-value of 0.05348 (**Figure 6G**); r^2_{power} (**Figure 6A**) indicates 6.339 cm/kyr, and

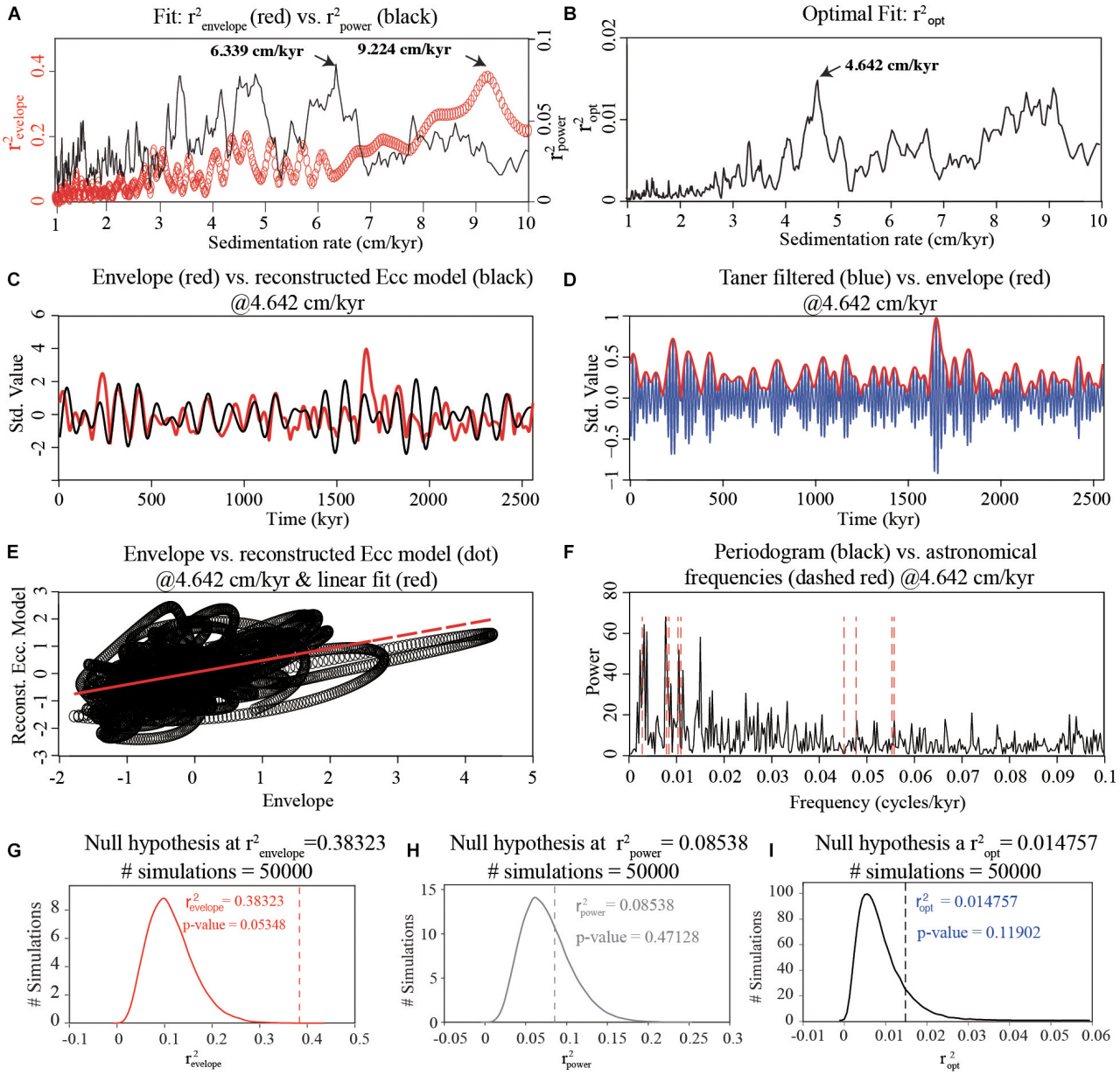

FIGURE 6 | TimeOpt **(A–F)** analysis and Monte Carlo simulation **(G–I)** results for the DBG MS series for 400 test sedimentation rates from 1 to 10 cm/kyr. The Taner filter passband was set to f_{low} = 0.045 cycles/kyr and f_{high} = 0.069 cycles/kyr; the roll-off was set to 10^{12}. The input orbital eccentricity model frequencies and precession index frequencies are from the La2004 solution (**Table 1**). **(A)** Pearson correlation coefficient vs. test sedimentation rate for the amplitude envelope of the precession index band ($r^2_{envelope}$) and eccentricity model (r^2_{power}). **(B)** The combined Pearson correlation coefficient $r^2_{opt} = r^2_{envelope} \cdot r^2_{power}$ indicating an optimal sedimentation rate of 4.642 cm/kyr. **(C)**. Comparison of the precession band amplitude envelope (red) and eccentricity model (black) for the optimal sedimentation rate of 4.6416 cm/kyr. **(D)** Taner-filtered precession band and amplitude envelope. **(E)** Paired amplitude envelope and eccentricity model points illustrating the correlation at the optimal sedimentation rate of 4.642 cm/kyr. **(F)**. Unsmoothed power spectrum of the MS series evaluated as a time series at the optimal sedimentation rate of 4.642 cm/kyr. **(G)** 50000 Monte Carlo simulations of AR1 red noise at the sedimentation rate indicated by the amplitude envelope of the precession index band (9.224 cm/kyr; $r^2_{envelope}$ = 0.38323; p = 0.05348). **(H)** 50000 Monte Carlo simulations of AR1 red noise at the sedimentation rate indicated by the orbital eccentricity model (6.339 cm/kyr; r^2_{power} = 0.08538; p = 0.47128). **(I)** 50000 Monte Carlo simulations of AR1 red noise at the optimal sedimentation rate (4.6416 cm/kyr; r^2_{opt} = 0.014757, p = 0.11902).

a much higher p-value of 0.47128 (**Figure 6H**). Adopting 4.642 cm/kyr as the optimal sedimentation rate, the MS series has a periodogram with a strong orbital eccentricity signature (**Figure 6F**).

COCO/eCOCO Analysis

COCO analysis indicates three maxima at 3.32, 4.72, and 6.34 cm/kyr, the largest at 4.72 cm/kyr with a correlation coefficient value exceeding 0.4 (**Figure 7A**). All three

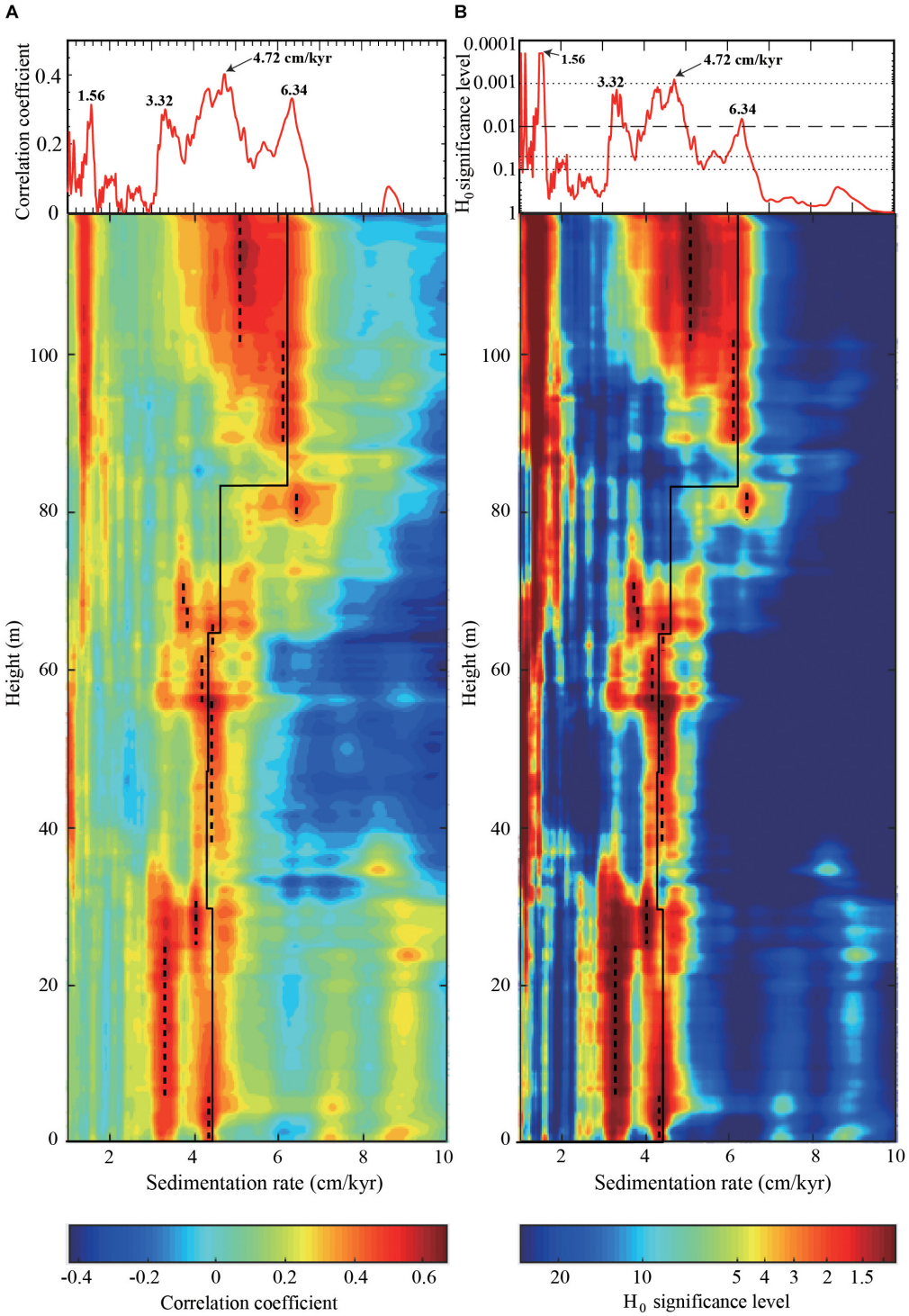

FIGURE 7 | Correlation coefficient (COCO) and evolutionary correlation coefficient (eCOCO) analysis of the DBG MS stratigraphic series. **(A)** Correlation coefficient vs. test sedimentation rate estimation of the correlation coefficient between the power spectra of astronomical solutions and the DBG MS series indicating an optimal sedimentation rate of 4.72 cm/kyr (top), and a sliding stratigraphic window to track variable sedimentation rates through the MS series (bottom). The vertical black lines indicate sedimentation rates according to the 405-kyr tuning (**Table 2**); the vertical dashed lines highlight the higher COCO values along the section. **(B)** The null hypothesis (H_0) significance level test (top) and evolutionary null hypothesis (H_0) significance level (bottom). For both the COCO and eCOCO, tested sedimentation rates range from 1 to 10 cm/kyr with a step of 0.02 cm/kyr, and the number of Monte Carlo simulations is 5000. For eCOCO analysis, the sliding window size is 38 m; the sliding window step is 0.02 m. In the top graph: the dashed horizontal line indicates $H_0 = 0.01$; the horizontal dotted lines, from top to bottom, indicate $H_0 = 0.001$, 0.05, and 0.1.

sedimentation rates have H_0 significance levels lower than 0.01 (**Figure 7B**). The results of eCOCO analysis shows that the sedimentation rates vary from 4.72 to 6.3 cm/kyr (**Figure 7A**).

DISCUSSION

Sedimentation Rate Variations in the DBG MS Series

The optimal sedimentation rates indicated by the ASM, TimeOpt and COCO methods are summarized in **Table 3**. Only one sedimentation rate is shared by all three methods: 4.642 cm/kyr (TimeOpt) to 4.72 cm/kyr (ASM, COCO). Other sedimentation rates arising at 3.4 and 6.34 cm/kyr can be explained as the result of sedimentation rate variations, as revealed by eCOCO (**Figure 7**). The TimeOpt precession index amplitude envelope model result indicating 9.224 cm/kyr (red circles, **Figure 6A**) with an extremely low *P*-value of 0.05348 (**Figure 6G**), is twice the joint optimal sedimentation rate of 4.642 cm/kyr that has a higher *P*-value of 0.11902, but shows an excellent fit of orbital eccentricity model frequencies in the periodogram (from 0 to 0.12 cycles/kyr) (**Figure 6F**). It is worth further considering this periodogram, and rescaling the frequencies by a factor of 2 (for 9.224 cm/kyr). This would shift the data spectral peaks that are currently at ∼100 kyr (0.01 cycles/kyr) to ∼50 kyr, and ∼400 kyr (0.0025 cycles/kyr) to ∼200 kyr, which do not coincide with the orbital eccentricity terms. Indeed, r^2_{power}, which compares the orbital eccentricity model and sedimentation rate-calibrated data, records a low value at 9.224 cm/kyr (**Figure 6A**). The joint modeling by r^2_{opt} steers the TimeOpt solution toward the sedimentation rate (4.642 cm/kyr) that produces a data periodogram with credible orbital eccentricity frequencies, and it is comparable to the sedimentation rate (4.72 cm/kyr) estimated by the other methods.

TABLE 2 | 405-kyr cycle and 100-kyr cycle picks (in bold and italic) based on MS minima in the MS stratigraphic series (see **Figure 2B**) that were identified with elevated statistical significance by the MTM harmonic F-ratio test (**Figure 4A**) and bandpass filters (**Figure 2D**).

Stratigraphic position (m)	Time (kyr)
0.0	***0***
3.92	98
20.06	503
36.18	908
54.44	1313
72.88	1718
97.84	2123
115.20	***2428***
117.82	***2478***

100-kyr cycle picks (in bold and italic) based on MS minima in the MS stratigraphic series.

TABLE 3 | Summary of sedimentation rates indicated by the ASM, TimeOpt, and COCO methods.

Method	Sedimentation rate (cm/kyr)			
ASM	3.339	4.723	–	–
TimeOpt/TimeOptSim	–	4.642	6.339	9.224
COCO	3.4	4.72	6.34	–

Astrochronology of the DBG MS Series

The astronomical frequencies identified in the DBG are supported by coeval evidence for astronomical forcing in the Valanginian–Hauterivian marine systems (e.g., Fiet et al., 2006; Martinez et al., 2015; Aguirre-Urreta et al., 2019). The optimization procedures reveal that the 20.5–16.4 m, 5.85–4.82 m, 3.28–1.42 m, and 0.98–0.75 m wavelengths in the MS stratigraphic series are associated with the periodicities of the long and short orbital eccentricity, obliquity and precession index, respectively.

Notably, assuming that the 16–20 m thick MS cycles along the section are 405 kyr cycles indicates sedimentation rates that are closely aligned with the objective testing (**Figure 7**: vertical dashed and solid black lines in the eCOCO color maps). The recognition of 405-kyr cycles is important for the ongoing initiative to define cyclostratigraphy in terms of the 405-kyr g_2-g_5 orbital eccentricity metronome for the geologic time scale (Kent et al., 2018; Hinnov, 2018). Applying the 405-kyr-based chronology model (**Table 2**) to convert the DBG MS stratigraphic series to a time series results in a spectrum with power concentrated in the short orbital eccentricity (influenced in part by three 100-kyr scale time points in **Table 2**), obliquity [1/(40.9 kyr), 1/(36.9 kyr) and 1/(27.6 kyr)] and precession index [1/(22.1 kyr) and 1/(18.9 kyr)] bands (**Figure 4C**). The spectrogram of the 405-kyr tuned MS series also indicates that the long and short orbital eccentricity trade positions in dominance at ∼400–500 kyr intervals along the section (**Figure 4D**).

The DBG MS cyclostratigraphy and the La2004 astronomical solution from 135 to 130 Ma are shown together in **Figure 8**. The yellow shading indicates a proposed correlation interval between data and model, from 133.265 to 130.787 Ma. This specific correlation was selected according to the singular coincidence at 131.538 Ma of an obliquity maximum and an orbital eccentricity minimum in both the La2004 astronomical solution and the 405-kyr tuned DBG time series (green vertical line in **Figure 8**). The obliquity-filtered DBG series (**Figure 8D**) also shows a pronounced amplitude modulation cycle that repeats every 6–7 cycles, which could be evidence for the recently described 173-kyr s_3–s_6 metronome, that is also present in the La2004 obliquity (**Figure 8B**; Boulila et al., 2018; Hinnov, 2018).

Paleoclimate Implications: The Weissert Event

The Weissert Event, characterized by a positive marine $d^{13}C$ excursion and global cooling, is the first major Early Cretaceous Earth system perturbation in the geologic record (Erba et al., 2004; Gröcke et al., 2005; Gréselle et al., 2011; Föllmi, 2012; Bajnai et al., 2017; Price et al., 2018). It is thought to span as much as 5.85 Myr (135.22–129.37 Ma) from the start of the Late Valanginian to the end of the Early Hauterivian (Martinez et al., 2015).

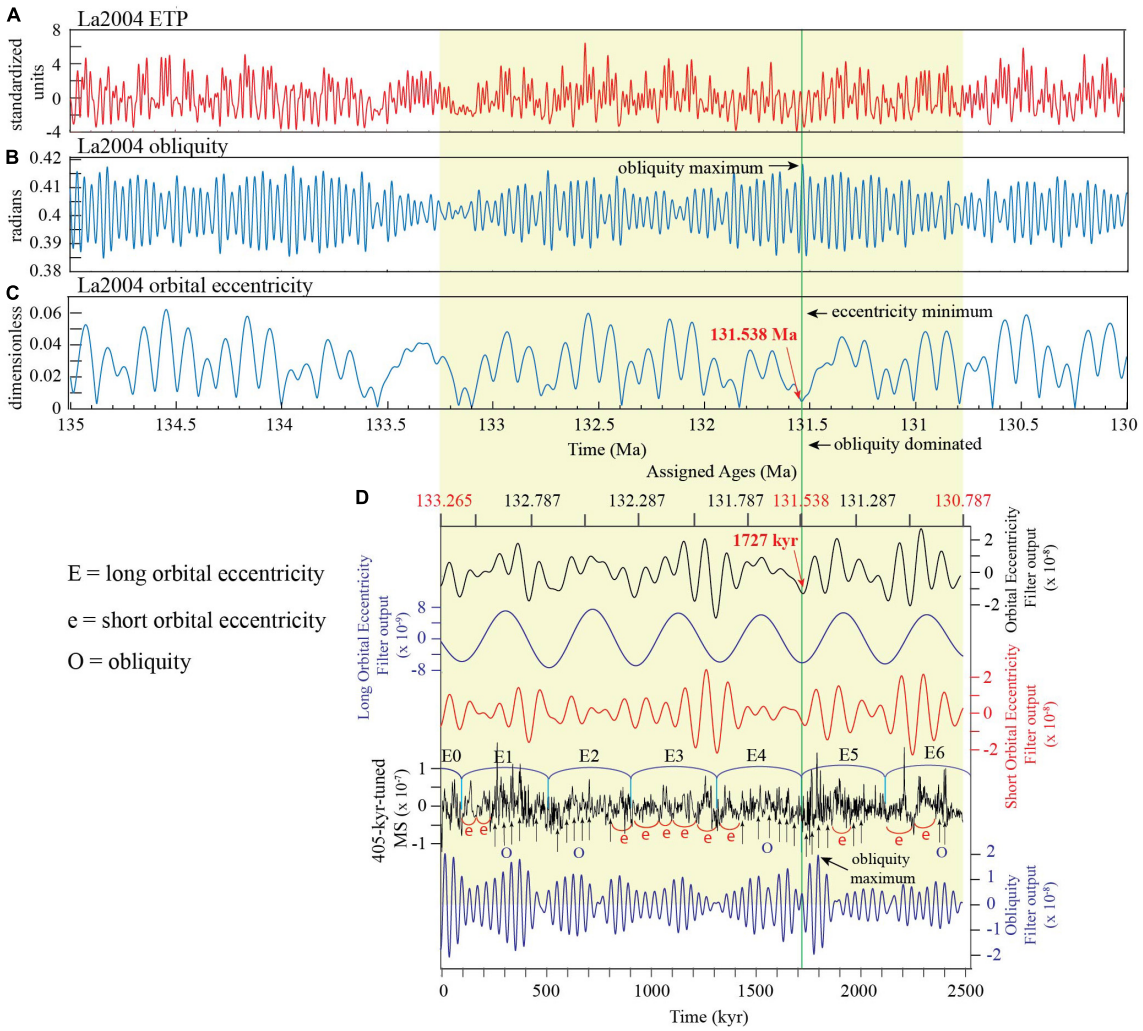

FIGURE 8 | Proposed correlation between DBG MS cyclostratigraphy and the La2004 astronomical solution from 135 to 130 Ma. The yellow shading indicates the proposed correlation interval, from 133.265 to 130.787 Ma; the green vertical line indicates a confluence of minimum orbital eccentricity and maximum obliquity in the La2004 solution. **(A)** La2004 ETP computed by standardizing and adding together the orbital eccentricity, obliquity and precession index solutions, producing a model with equal variance contributions from all three astronomical parameters. **(B)** The La2004 obliquity variation. **(C)** The La2004 orbital eccentricity solution. **(D)** The 405-kyr-tuned DBG MS time series, from the top: orbital eccentricity bandpass-filtered time series; 405-kyr (long orbital eccentricity) bandpass-filtered time series (E0-E6 are as in **Figure 2**); ∼100 kyr (short orbital eccentricity) bandpass-filtered time series; the Taner-highpass-filtered time series (see Preprocessing); and ∼37-kyr (obliquity) bandpass-filtered time series.

By this measure, the DBG, from 133.265 to 130.787 Ma (**Figure 8**), falls entirely within the Weissert Event. Geochemical analysis of the DBG indicates that the formation was deposited under relatively low-intensity hinterland weathering related to the boreal or semiarid regions; the upper unit of the DBG records hinterland weathering that is comparable to that in temperate and humid mid-latitude regions (Ohta et al., 2011). Palynoflora data also indicate that the paleoclimate changed from semi-humid to relatively temperate and humid conditions during DBG time (Wang et al., 2016).

The change toward more humid conditions during the late Berriasian and intensification during the Valanginian Weissert Event evidently influenced terrestrial biota, and especially the evolution of herbivore vertebrates. A study of oxygen isotope composition of vertebrate apatite in Liaoning Province, China, indicates global cooling during Jehol Biota time, demonstrated by an estimated air temperature of 10 ± 4°C (Amiot et al., 2011). Zhou (2014) also found temperate-to-cool-temperate fossil wood genus *Xenoxylon* in the Jehol Lagerstätte and an absence of crocodilians in northeastern China.

CONCLUSION

The DBG in the LPB, Hebei Province, northeastern China represents the prelude to the Jehol Biota, the spectacular Lagerstätte in the Lower Cretaceous. However, the DBG also occurs in a geologic interval that is chronostratigraphically very

poorly constrained. This state of affairs motivated measuring the DBG for MS to search for astronomical signals during DBG time, with the larger goal of developing an astrochronology for the formation. The results are as followings:

- A high-resolution (2 cm measuring interval) MS stratigraphic series was collected from the predominantly cyclic continental (lacustrine) DBG of the Yushuxia section in Luanping Basin, NE China.
- Gamma ray (GR) data indicate that MS increases with detrital content of the sediment, linking MS to fluvial delivery of sediment to the LPB, the hydrologic cycle, and climate forcing.
- Spectral analysis of the DBG MS stratigraphic series indicates that cyclicity occurs at wavelengths of 16.38 m, 5.85–4.82 m, 3.28–1.42 m, and 0.98–0.75 m. These are proposed to represent long orbital eccentricity, short orbital eccentricity, obliquity and precession index cycles.
- Objective testing using ASM, TimeOpt/TimeOptSim and COCO/eCOCO indicates the presence of Early Cretaceous (∼132.05 Ma) astronomical frequencies predicted by the La2004 astronomical solution. The testing identifies common optimal sedimentation rates of 4.642–4.72 cm/kyr measured by all three methods.
- Correlation between the 405-kyr-tuned DBG MS time series and the La2004 astronomical solution, generally constrained by radioisotope dating, suggests that the DBG was deposited from 133.265 to 130.787 Ma with a duration of 2478 kyr.
- Strong correlation between the DBG MS-La2004 astronomical solution raises the possibility that the La2004 solution is valid much further back in time than is currently recognized.
- The global cooling Weissert Event lasted from 135.22 to 129.37 Ma, indicating that DBG deposition, and hence, early stage Jehol Biota, occurred entirely within the Weissert Event.

DATA AVAILABILITY STATEMENT

The raw data supporting the conclusions of this article will be made available by the authors, without undue reservation, to any qualified researcher.

AUTHOR CONTRIBUTIONS

HW designed the study. WL measured the data and performed the analysis and modeling. WL, LH, and HW wrote the manuscript. All authors contributed to data interpretation and provided significant input to the final manuscript.

FUNDING

This work was supported by the National Natural Science Foundation of China (41790451, 41925010, and 41688103), the National Key R&D Program of China (2019YFC0605403), and the Chinese "111" project (B20011).

ACKNOWLEDGMENTS

We express our sincere thanks to associate editor Prof. Juan C. Larrasoaña, guest editors Profs. Kenneth Philip Kodama and Luigi Jovane. We thank two reviewers for their careful review and constructive suggestions that significantly improved the manuscript. We also thank Zuohuan Qin, Jichuang Fang, Wenjun Cai, and Chengke He for their help in the field.

SUPPLEMENTARY MATERIAL

The Supplementary Material for this article can be found online at: https://www.frontiersin.org/articles/10.3389/feart.2020.00178/full#supplementary-material

REFERENCES

Aguirre-Urreta, B., Martinez, M., Schmitz, M., Lescano, M., Omarini, J., Tunik, M., et al. (2019). Interhemispheric radio-astrochronological calibration of the time scales from the andean and the tethyan areas in the valanginian-hauterivian (Early Cretaceous). *Gondwana Res.* 70, 104–132. doi: 10.1016/j.gr.2019.01.006

Amiot, R., Wang, X., Zhou, Z. H., Wang, X. L., Buffetaut, E., Lécuyer, C., et al. (2011). Oxygen isotopes of East Asian dinosaurs reveal exceptionally cold Early Cretaceous climates. *Proc. Natl. Acad. Sci. U.S.A.* 108, 5179–5183. doi: 10.1073/pnas.1011369108

Bajnai, D., Pálfy, J., Martinez, M., Price, G. D., Nyerges, A., and Fõzy, I. (2017). Multi-proxy record of orbital-scale changes in climate and sedimentation during the weissert event in the valanginian bersek marl formation (Gerecse Mts., Hungary). *Cretaceous Res* 75, 45–60. doi: 10.1016/j.cretres.2017.02.021

Boulila, S., Vahlenkamp, M., De Vleeschouwer, D., Laskar, J., Yamamoto, Y., Pälike, H., et al. (2018). Towards a robust and consistent middle Eocene astronomical timescale. *Earth Planet. Sci. Lett.* 486, 94–107. doi: 10.1016/j.epsl.2018.01.003

Chang, S. C., Zhang, H. C., Renne, P. R., and Fang, Y. (2009). High-precision 40Ar/39Ar age for Jehol Biota. *Palaeogeogr. Palaeoclimatol. Palaeoecol.* 280, 94–104. doi: 10.1016/j.palaeo.2009.06.021

Crain, E. R. (2019). Avaliable at: www.spec2000.net. (accessed December 31, 2019).

Erba, E., Bartolini, A., and Larson, R. (2004). Valanginian Weissert oceanic anoxic event. *Geology* 32, 149–152. doi: 10.1130/G20008.1

Fiet, N., Quidelleur, X., Parize, O., Bulot, L. G., and Gillot, P. Y. (2006). Lower Cretaceous stage durations combining radiometric data and orbital chronology: towards a more stable relative time scale? *Earth Planet. Sci. Lett.* 246, 407–417. doi: 10.1016/j.epsl.2006.04.014

Föllmi, K. B. (2012). Early Cretaceous life, climate and anoxia. *Cretaceous Res.* 35, 230–257. doi: 10.1016/j.cretres.2011.12.005

Gao, L. Z., Wang, Y. S., and Zhang, H. (2018). A discussion on Jurassic and Cretaceous boundary based on the SHRIMP zircon U-Pb dating of Mesozoic holitype section in Luanping basin. *Geol. Bull. China* 37, 1186–1192.

Gréselle, B., Pittet, B., Mattioli, E., Joachimski, M., Barbarin, N., Riquier, L., et al. (2011). The Valanginian isotope event: a complex suite of palaeoenvironmental perturbations. *Palaeogeogr. Palaeoclimatol. Palaeoecol.* 306, 41–57. doi: 10.1016/j.palaeo.2011.03.027

Gröcke, D. R., Price, G. D., Robinson, S. A., Baraboshkin, E. Y., Mutterlose, J., and Ruffell, A. H. (2005). The upper valanginian (Early Cretaceous) positive carbon-isotope event recorded in terrestrial plants. *Earth Planet. Sci. Lett.* 240, 495–509. doi: 10.1016/j.epsl.2005.09.001

He, H. Y., Wang, X. L., Zhou, Z. H., Jin, F., Wang, F., Yang, K. L., et al. (2006). The 40Ar/39Ar dating of the early jehol biota from fengning, hebei province, northern China. *Geochem. Geophys. Geosyst.* 7:Q04001. doi: 10.1029/2005GC001083

Hinnov, L. A. (2018). "Chapter 1: cyclostratigraphy and Astrochronology in 2018," in *Stratigraphy and Timescales*, Vol. 3, ed. M. Montenari (Cambridge, MA: Academic Press), 1–80. doi: 10.1016/bs.sats.2018.08.004

Huang, C. J. (2018). "Chapter two: astronomical time scale for the mesozoic," in *Stratigraphy and Timescales* ed M. Montenari. (Cambridge, MA: Academic Press)3, 81–150. doi: 10.1016/bs.sats.2018.08.005

Huang, D. Y., Cai, C. Y., Jiang, J. Q., Su, Y. T., and Liao, H. Y. (2015). Daohugou bed and fossil of its basal conglomerate section. *Acta Palaeontol. Sin.* 54, 351–357.

Huang, Z. H., Boyd, R., and O'Connell, S. B. (1992). "Upper Cretaceous cyclic sediments from hole 762C, exmouth plateau, Northwest Australia," in *Proceedings of the Ocean Drilling Program, Scientific Results*, Vol. 122, eds U. Van Rad, B. U. Haq, (College Station, TX: Ocean Drilling Program), 259–277.

Kent, D. V., Olsen, P. E., Rasmussen, C., Lepre, C., Mundil, R., Irmis, R. B., et al. (2018). Empirical evidence for stability of the 405 kyr Jupiter-Venus eccentricity cycle over hundreds of millions of years. *Proc. Natl. Acad. Sci. U.S.A.* 115, 6153–6158. doi: 10.1073/pnas.1800891115

Ji, Q., Liu, Y. Q., Ji, S. A., Chen, W., Lv, J. C., You, H. L., et al. (2006). On the terrestrial Jurassice-Cretaceous Boundary in China. *Geol. Bull. China* 25, 336–339. doi: 10.3969/j.issn.1671-2552.2006.03.003

Kodama, K. P. (2012). *Paleomagnetism of Sedimentary Rocks: Process and Interpretation*. Chichester: John Wiley and Sons, 157.

Kodama, K. P. (2019). Rock magnetic cyclostratigraphy of the carboniferous mauch chunk formation, Pottsville, PA, United States. *Front. Earth Sci.* 7:285. doi: 10.3389/feart.2019.00285

Kodama, K. P., and Hinnov, L. A. (2015). *Rock Magnetic Cyclostratigraphy*. Chichester: Wiley Blackwell, 165.

Laskar, J., Fienga, A., Gastineau, M., and Manche, H. (2011a). La2010: a new orbital solution for the long-term motion of the earth. *Astron. Astrophys* 532:A89. doi: 10.1051/0004-6361/201116836

Laskar, J., Gastineau, M., Delisle, J. B., Farrés, A., and Fienga, A. (2011b). Strong chaos induced by close encounters with Ceres and Vesta. *Astron. Astrophys.* 532:L4. doi: 10.1051/0004-6361/201117504

Laskar, J., Robutel, P., Joutel, F., Gastineau, M., Correia, A. C. M., and Levrard, B. (2004). A long-term numerical solution for the insolation quantities of the Earth. *Astron. Astrophys* 428, 261–285. doi: 10.1051/0004-6361:20041335

Li, M. S., Hinnov, L. A., and Kump, L. R. (2019). Acycle: time-series analysis software for paleoclimate research and education. *Comput. Geosci.* 127, 12–22. doi: 10.1016/j.cageo.2019.02.011

Li, M. S., Kump, L. R., Hinnov, L. A., and Mann, M. E. (2018). Tracking variable sedimentation rates and astronomical forcing in Phanerozoic paleoclimate proxy series with evolutionary correlation coefficients and hypothesis testing. *Earth Planet. Sci. Lett.* 501, 165–179. doi: 10.1016/j.epsl.2018.08.041

Li, P. X., Liu, Y. Q., and Tian, S. G. (2004). Advances in the study of the Jurassic–Cretaceous lithostratigraphy in the Luanping basin, northern Hebei. *Geol. Bull. China* 23, 757–765. doi: 10.3969/j.issn.1671-2552.2004.08.006

Liu, W., Wu, H. C., Hinnov, L. A., Baddouh, M., Wang, P. J., Gao, Y. F., et al. (2020). An 11 million-year-long record of astronomically forced fluvial-alluvial deposition and paleoclimate change in the Early Cretaceous songliao synrift basin, China. *Palaeogeogr. Palaeoclimatol. Palaeoecol.* 541:109555. doi: 10.1016/j.palaeo.2019.109555

Liu, Y. Q., Li, P. X., and Tian, S. G. (2003). SHRIMP U-Pb zircon age of Late Mesozoic tuffs (lava) in Luanping basin, northern Hebei, and its implications. *Acta Petrologica Mineralogical.* 22, 237–244. doi: 10.3969/j.issn.1000-6524.2003.03.005

Liu, Y. Q., Pang, Q. Q., Li, P. X., Tian, S. G., and Niu, S. W. (2002). Advances in the study of non-marine jurassic Cretaceous biostratigraphical boundary and candidate stratotype in Luanping basin, northern Hebei. *Geol. Bull. China* 21, 176–180. doi: 10.3969/j.issn.1671-2552.2002.03.015

Liu, Y. Q., Tian, S. G., Li, P. X., Pang, Q. Q., and Li, Y. (2001). The stratigraphic framework of the dabeigou-dadianzi formations in luanping basin, Northern Hebei and its stratotype significance. *Acta Geosci. Sin.* 22, 391–396.

Ma, C., Meyers, S. R., and Sageman, B. B. (2017). Theory of chaotic orbital variations confirmed by Cretaceous geological evidence. *Nature* 542, 468–470. doi: 10.1038/nature21402

Ma, C., Meyers, S. R., and Sageman, B. B. (2019). Testing late cretaceous astronomical solutions in a 15 million year astrochronologic record from North America. *Earth Planet. Sci. Lett.* 513, 1–11. doi: 10.1016/j.epsl.2019.01.053

Martinez, M., Deconinck, J. F., Pellenard, P., Riquier, L., Company, M., Reboulet, S., et al. (2015). Astrochronology of the valanginian-hauterivian stages (Early Cretaceous): chronological relationships between the Paraná-Etendeka large igneous province and the Weissert and the Faraoni events. *Global Planet. Change* 131, 158–173. doi: 10.1016/j.gloplacha.2015.06.001

Mayer, H., and Appel, E. (1999). Milankovitch cyclicity and rock-magnetic signatures of paleoclimatic changes in the Early Cretaceous Biancone Formation of the Southern Alps. Italy. *Cretaceous Res.* 20, 189–214. doi: 10.1006/cres.1999.0145

Meyers, S. R. (2014). *Astrochron: An R Package for Astrochronology*. Avaliable at: https://cran.r-project.org/package=astrochron

Meyers, S. R. (2015). The evaluation of eccentricity-related amplitude modulation and bundling in paleoclimate data: an inverse approach for astrochronologic testing and time scale optimization. *Paleoceanography* 30, 1625–1640. doi: 10.1002/2015PA002850

Meyers, S. R. (2019). Cyclostratigraphy and the problem of astrochronologic testing. *Earth Sci. Rev.* 190, 190–223. doi: 10.1016/j.earscirev.2018.11.015

Meyers, S. R., and Malinverno, A. (2018). Proterozoic milankovitch cycles and the history of the solar system. *Proc. Natl. Acad. Sci. U.S.A.* 115, 6363–6368. doi: 10.1073/pnas.1717689115

Meyers, S. R., and Sageman, B. B. (2007). Quantification of deep-time orbital forcing by average spectral misfit. *Am. J. Sci.* 307, 773–792. doi: 10.2475/05.2007.01

Niu, S. W., Sun, C. L., Zhang, F. C., Li, W. G., Xu, F., Li, H., et al. (2015). Local fossil assemblage of the Jehol biota and its geological significance in Chengde area. Hebei Province, China. *Geol. Surv. Res.* 38, 241–247.

Niu, S. W., Tian, S. G., and Pang, Q. Q. (2010). Conchostracan biostratigraphy of the dadianzi formation in the luanping basin, northern Hebei, China and the boundary of continental Jurassic and Cretaceous strata. *Geol. Bull. China* 29, 961–979.

Ohta, T., Li, G., Hirano, H., Sakai, T., Kozai, T., Yoshikawa, T., et al. (2011). Early Cretaceous terrestrial weathering in Northern China: relationship between paleoclimate change and the phased evolution of the jehol biota. *J. Geol.* 119, 81–96. doi: 10.1086/657341

Pei, J. L., Yang, Z. Y., Sun, Z. M., Tong, Y. B., Cai, Y. H., Wang, X. R., et al. (2019). Magnetostratigraphic dating of the early jehol biota. *Acta Geosci. Sin.* 40, 393–404.

Price, G. D., Janssen, N. M. M., Martinez, M., Company, M., Vandevelde, J. H., and Grimes, S. T. (2018). A High-Resolution belemnite geochemical analysis of early Cretaceous (Valanginian-Hauterivian) environmental and climatic perturbations. *Geochem. Geophys. Geosyst.* 19, 3832–3843. doi: 10.1029/2018GC007676

Qin, Z. H., Xi, D. P., Sames, B., Do Carmo, D. A., Wang, X. R., Xu, K. K., et al. (2018). Ostracods of the non-marine lower Cretaceous dabeigou formation at yushuxia (Luanping basin, North China): implications for the early Jehol Biota age. *Cretaceous Res.* 86, 199–218. doi: 10.1016/j.cretres.2018.03.010

Swisher, C. C., Wang, X. L., Zhou, Z. H., Wang, Y. Q., Jing, F., Zhang, J. Y., et al. (2002). Further support for a Cretaceous age for featured dinosaur beds of liaoning province, China: new 40Ar/39Ar dating of the Yixian and Tuchengzi formations. *Chin. Sci. Bull.* 47, 135–138.

Swisher, C. C., Wang, Y. Q., Wang, X. L., Xu, X., and Wang, Y. (1999). Cretaceous age for the feathered dinosaurs of Liaoning. China. *Nature* 400, 59–61. doi: 10.1038/21872

Thomson, D. (1982). Spectrum estimation and harmonic analysis. *Proc. IEEE* 70, 1055–1096. doi: 10.1109/PROC.1982.12433

Tian, S. G., Niu, S. W., and Pang, Q. Q. (2008). Redefinition of the lower Cretaceous terrestrial Yixianian Stage and its stratotype candidate in the Luanping basin, northern Hebei. *Geol. Bull. China* 27, 739–752. doi: 10.3969/j.issn.1671-2552.2008.06.003

Tian, S. G., Pang, Q. Q., Niu, S. W., Li, P. X., and Liu, Y. Q. (2004). Terrestrial Jurassic-Cretaceous stratotype candidate in Luanping basin, northern Hebei. *Geol. Bull. China* 23, 1170–1179. doi: 10.3969/j.issn.1671-2552.2004.12.002

Wan, X. Q., Gao, F. L., Qin, Z. H., Cui, C., and Xi, D. P. (2016). The Jurassic-Cretaceous boundary problem and the discussion on continental boundary of northern China. *Geosci. Front.* 23, 1–6.

Wang, C. S. (2013). Environmental/climate change in the Cretaceous greenhouse world: records from Terrestrial scientific drilling of songliao basin and adjacent areas of China. *Palaeogeogr. Palaeoclimatol. Palaeoecol.* 385, 1–5. doi: 10.1016/j.palaeo.2013.05.006

Wang, C. S., Feng, Z. Q., Zhang, L. M., Huang, Y. J., Cao, K., Wang, P. J., et al. (2013). Cretaceous paleogeography and paleoclimate and the setting of SKI borehole sites in Songliao Basin, northeast China. *Palaeogeogr. Palaeoclimatol. Palaeoecol* 385, 17–30. doi: 10.1016/j.palaeo.2012.01.030

Wang, S. E., Gao, L. Z., Wan, X. Q., and Song, B. (2013). Ages of Tuchengzi Formation in western Liaoning-northern Hebei area in correlation with those of international strata. *Geol. Bull. China* 32, 1673–1690. doi: 10.3969/j.issn.1671-2552.2013.11.001

Wang, D. N., Wang, X. R., and Ji, Q. (2016). The Palynoflora alternation and the paleoclimate change at the turning time between Late Jurassic and Early Cretaceous in Northern Hebei and Western Liaoning. *Acta Geosci. Sin.* 37, 449–459. doi: 10.3975/cagsb.2016.04.07

Wang, S. E., and Ji, Q. (2009). Lithostratigraphy and biostratigraphy features of zhangjiakou formation and dabeigou formation and its significance for stratigraphic subdivision and correlation in the Northeast Asia. *Geol. Bull. China* 28, 821–828.

Wang, Y. Q., Sha, J. G., Pan, Y. H., and Zhang, X. L. (2015). Early Cretaceous nonmarine ostracod biostratigraphy of western Liaoning area. NE China. *Micropaleontology* 61, 135–145. doi: 10.1002/rcm.2049

Wu, F. D., Chen, Y. J., Hou, Y. A., Zhang, F., and Li, U. (2004). Characteristics of sedimentary tectonic evolution and high-resolution sequence stratigraphy in luanping basin. *Earth Sci. J. China Unive. Geosci.* 29, 625–630.

Wu, H. C., Zhang, S. H., Hinnov, L. A., Jiang, G. Q., Yang, T. S., Li, H. Y., et al. (2014). Cyclostratigraphy and orbital tuning of the terrestrial upper Santonian-Lower Danian in Songliao Basin, northeastern China. *Earth Planet. Sci. Lett.* 407, 82–95. doi: 10.1016/j.epsl.2014.09.038

Wu, H. C., Zhang, S. H., Jiang, G. Q., Hinnov, L. A., Yang, T. S., Li, H. Y., et al. (2013a). Astrochronology of the early turonian-early campanian terrestrial succession in the songliao basin, northeastern China and its implication for long-period behavior of the Solar System. *Palaeogeogr. Palaeoclimatol. Palaeoecol.* 385, 55–70. doi: 10.1016/j.palaeo.2012.09.004

Wu, H. C., Zhang, S. H., Jiang, G. Q., Yang, T. S., Guo, J. H., and Li, H. Y. (2013b). Astrochronology for the Early Cretaceous Jehol Biota in Northeastern China. *Palaeogeogr. Palaeoclimatol. Palaeoecol.* 385, 221–228. doi: 10.1016/j.palaeo.2013.05.017

Wu, H. C., Zhang, S. H., Jiang, G. Q., and Huang, Q. H. (2009). The floating astronomical time scale for the terrestrial late Cretaceous Qingshankou formation from the Songliao Basin of Northeast China and its stratigraphic and paleoclimate implications. *Earth Planet. Sci. Lett.* 278, 308–323. doi: 10.1016/j.epsl.2008.12.016

Xi, D. P., Wan, X. Q., Li, G. B., and Li, G. (2019). Cretaceous integrative stratigraphy and timescale of China. *Sci. China: Earth Sci.* 62, 256–286. doi: 10.1007/s11430-017-9262-y

Xu, X., Zhou, Z., Wang, Y., and Wang, M. (2019). Study on Jehol Biota: recent advances and future prospects. *Sci. China: Earth Sci.* 49, 1491–1511. doi: 10.1360/SSTe-2019-0121

Yang, W., Li, S. G., and Jiang, B. Y. (2007). New evidence for Cretaceous age of the feathered dinosaurs of Liaoning: zircon U-Pb SHRIMP dating of the Yixian Formation in Sihetun, northeast China. *Cretaceous Res.* 28, 177–182. doi: 10.1016/j.cretres.2006.05.011

Zeebe, R. E., and Lourens, L. (2019). Solar System chaos and the Paleocene-Eocene boundary age constrained by geology and astronomy. *Nature* 365, 926–929. doi: 10.1126/science.aax0612

Zhang, H., Liu, X. M., Zhang, Y. Q., Yuan, H. L., and Hu, Z. C. (2005). Zircon U-Pb ages and significance of bottom and top beds of Zhangjiakou Formation in Liaoning and Hebei Provinces. *Earth Science-Journal of China University of Geosciences* 30, 387–401.

Zhang, Y. L., Qu, H. J., and Meng, Q. R. (2007). Depositional process and evolution of Luanping Early Cretaceous basin in the Yanshan structural belt. *Acta Petrol. Sin.* 23, 667–678. doi: 10.3321/j.issn:1000-0569.2007.03.013

Zhong, Y. Y., Wu, H. C., Zhang, Y. D., Zhang, S. H., Yang, T. S., Li, H. Y., et al. (2018). Astronomical calibration of the middle ordovician of the yangtze block, South China. *Palaeogeogr. Palaeoclimatol. Palaeoecol.* 505, 86–99. doi: 10.1016/j.palaeo.2018.05.030

Zhou, Z. H. (2014). The Jehol biota, an early Cretaceous terrestrial Lagerstätte: new discoveries and implications. *Natl. Sci. Rev.* 1, 543–559. doi: 10.1093/nsr/nwu055

Zhou, Z. H., Barrett, P. M., and Hilton, J. (2003). An exceptionally preserved lower Cretaceous ecosystem. *Nature* 421, 807–814. doi: 10.1038/nature01420

Zhou, Z. H., He, H. Y., and Jiang, X. L. (2009). The continental Jurassic-Cretaceous boundary in China. *Acta Palaeontol. Sin.* 48, 541–555.

Conflict of Interest: The authors declare that the research was conducted in the absence of any commercial or financial relationships that could be construed as a potential conflict of interest.